Supporting Information for:

# Inducing Structural Diversity in Anionic Metal–Tetraoxolene Coordination Polymers Using Templating Methyl Viologen Countercations

Martin P. van Koeverden[†], Brendan F. Abrahams[*], Carol Hua[‡], Timothy A. Hudson, Richard Robson

School of Chemistry, The University of Melbourne, Parkville, Victoria 3010, Australia

† Present Address: School of Chemistry, The University of Sydney, Sydney, NSW 2006, Australia.

‡ Present Address: School of Life and Environmental Sciences, Deakin University, Waurn Ponds, VIC 3216, Australia

*Email: bfa@unimelb.edu.au

## Table of Contents

## Experimental

### General Considerations

Anhydrous MeCN was obtained by drying MeCN twice sequentially over activated 3 Å molecular sieves, which was then stored under an atmosphere of dry $N_2$. Proton ($^1$H) and proton-decoupled carbon-13 ($^{13}$C{$^1$H}) NMR spectroscopy was performed using a Varian Unity spectrometer operating at 400 and 100 MHz respectively. All spectra were acquired at 25 °C. Proton ($\delta_H$) and carbon-13 ($\delta_C$) chemical shift values are reported in parts per million (ppm) downfield of external tetramethylsilane. $^1$H- and $^{13}$C{$^1$H}-NMR spectra were referenced to residual $^1$H signals in the deuterated solvents and the solvent signal respectively, except for spectra acquired in $D_2O$ which were referenced to the $^1$H and $^{13}$C signals of acetone (internal standard, $\delta_H$ 2.22; $\delta_C$ 215.94). Thermogravimetric analysis (TGA) was performed using a Mettler Toledo TGA/SDTA851e between 25 °C and 450 °C using a heating rate of 5 °C min$^{-1}$ in a flow of $N_2$. Fourier-transform infrared (FT-IR) spectra were recorded in air under ambient conditions using either a Bruker Tensor 27 FTIR spectrometer (KBr discs), or a Perkin Elmer Spotlight 100 spectrometer fitted with a ZnSe Universal ATR accessory. Elemental analyses (CHN) were performed at the Campbell Microanalytical Laboratory, University of Otago.

### 3,6-Difluoro-2,5-dihydroxy-1,4-benzoquinone (Fluoranilic acid, H₂Fan)

H₂Fan was synthesised using a modified literature procedure[1] in two steps from commercially available 2,3,5,6-tetrafluorohydroquinone, via the intermediate 2,3,5,6-tetrafluoro-1,4-benzoquinone (F₄BQ), also obtained using a modified literature procedure.[2] In brief, $(NH_4)_2Ce^{IV}(NO_3)_6$ (145.1 g, 220 mmol) was dissolved with stirring in $H_2O$ (700 mL). 2,3,5,6-Tetrafluorohydroquinone (18.21 g, 100 mmol) was added portion wise to the stirring $Ce^{IV}$ solution, causing an immediate colour change from a transparent orange solution to a pale-yellow suspension. The reaction was stirred 1 hr at rt., then extracted with $Et_2O$ (3 × 200 mL) until the organic extract was colourless. The combined organic phase was washed with $H_2O$ acidified with 2 drops conc. HCl (2 × 150 mL), brine acidified with 1 drop conc. HCl (150 mL), dried over $MgSO_4$ then concentrated to dryness at reduced pressure, yielding F₄BQ as a pale yellow scaly solid (15.63 g, 86.8%), which was used without further purification. FT-IR (KBr, cm$^{-1}$): 3442 (br s), 1702 (s), 1690 (s), 1677 (s), 1384 (m), 1335 (m), 1266 (w), 1004 (m), 542 (br w).

NaOH (9.5582 g, 734 mmol) was dissolved in $H_2O$ (190 mL) and cooled in an ice-water bath to <10 °C. F₄BQ (9.5582 g, 53.1 mmol) dissolved in 1,4-dioxane (75 mL) was added dropwise over 30 min to the vigorously stirring NaOH solution. The reaction was then stirred 30 min at 10 °C, then warmed to 60 °C and stirred 1 hr. The chocolate brown suspension was cooled to rt., then the solids isolated by suction filtration (Por. 3 frit). The product was washed on the frit with 10% w/w NaOH solution (2 × 75 mL), 1:1 v/v EtOH/$H_2O$ (100 mL) then EtOH (100 mL). The chocolate brown solid was then dried 24 hrs at 100 °C yielding an olive-green crude of Na₂Fan (10.51 g). The crude Na₂Fan (10.51 g) was suspended in $H_2O$ (300 mL) and heated to 60 °C with stirring. Conc. HCl (100 mL) was added dropwise to the stirring suspension, causing precipitation of a dark red crystalline product. The reaction was cooled to rt., then the precipitated solids isolated by suction filtration (Por. 3 frit), then dried by suction yielding an orange-red crude (6.4468 g). The crude was dissolved in the minimum of boiling AcOH

(120 mL), hot filtered to remove trace brown residue, then concentrated by boiling to ca. 80 mL. The intense cherry-red solution was then cooled slowly to rt. The crystallised orange-red rods were isolated by suction filtration (Por. 3 frit), dried by suction then washed with *n*-hexane (2 × 100 mL), then dried *in vacuo* (0.3 mbar, 80 °C) over KOH yielding the title compound as a bright orange powder (4.88 g, 52.2% from F$_4$BQ). FT-IR (KBr, cm$^{-1}$): 3585 (br s), 3477 (br s), 1673 (m), 1631 (s), 1452 (w), 1384 (w), 1303 (m), 998 (m), 606 (br w).

### 3,6-Difluoro-1,2,4,5-tetrahydroxybenzene (H$_4$Fan)

3,6-Difluoro-1,2,4,5-tetrahydroxybenzene (H$_4$Fan) was synthesised according to a modified literature procedure.[3] In air, H$_2$Fan (4.2420 g, 24.1 mmol) was suspended in conc. HCl (100 mL) then heated to 100 °C with stirring. Mossy tin (3.433 g, 28.9 mg-atom) was added portion wise over 5 minutes to the stirring orange-red suspension, causing gas evolution and gradual bleaching of the solution. After 30 min., the clear pale-yellow solution was hot filtered through glass fibre paper to remove traces of insoluble tan residue and unreacted Sn. The clear filtrate was cooled slowly to rt., then 4 °C overnight. The crystallised pale-tan needles were isolated by suction filtration (Por. 3 frit) under an N$_2$ stream, then washed on the frit with conc. HCl (2 × 30 mL), dried by suction in a brisk N$_2$ stream, then washed on the frit with ice-cold CHCl$_3$ (2 × 30 mL). The product was then dried *in vacuo* over KOH then P$_2$O$_5$, yielding the title compound as pale-tan needles (3.77 g, 87.9%). The product is stable over several months when stored under N$_2$ at 4 °C. FT-IR (ATR, cm$^{-1}$): 3525 (br m), 3373 (br m), 3211 (br m), 1648 (m), 1546 (w), 1532 (w), 1498 (s), 1405 (w), 1327 (m), 1294 (w), 1235 (w), 1207 (m), 988 (m), 955 (s), 703 (w), 635 (w), 608 (w).

### 3,6-Dichloro-1,2,4,5-tetrahydroxybenzene (H$_4$Clan)

H$_4$Clan was synthesised using a modified literature procedure.[3] In air, chloranilic acid (H$_2$Clan, 6.270 g, 30 mmol) was suspended in concentrated HCl (150 mL) then heated to 100 °C with stirring. Mossy tin (4.271 g, 36 mg-atom) was added portion wise over 5 minutes to the stirring red-orange suspension, causing gas evolution, and gradual bleaching of the solution. After 20 min., the clear pale-yellow reaction solution was hot filtered through glass fibre paper to remove traces of an insoluble tan residue and unreacted Sn, rinsing the reaction flask with additional hot concentrated HCl (2 × 20 mL). The clear filtrate was transferred to a flask fitted with a septum, purged with N$_2$ then cooled to rt. then 4 °C overnight. The product crystallised as white needles, which were isolated by suction filtration. The product was washed with ice-cold concentrated HCl (3 × 25 mL), then sucked dry and washed with ice-cold CHCl$_3$ (2 × 25 mL). The solid was dried *in vacuo* over KOH then P$_2$O$_5$, yielding the title compound as white to pale-tan needles (3.8505 g, 61.1%). The product is stable over several months when stored under dry N$_2$ at 4 °C. $^{13}$C{$^1$H}-NMR (100 MHz, $d_6$-Acetone): $\delta_C$ 137.3, 110.5. FT-IR (ATR, cm$^{-1}$): 3281 (s, br); 1632 (w); 1541 (w); 1466 (s); 1327 (m); 1288 (m); 1148 (s); 961 (s); 920 (m); 861 (m); 821 (s); 713 (m); 608 (m).

### *N,N′*-Dimethyl-4,4′-bipyridinium di(4-toluenesulfonate) [MeV(OTs)$_2$]

4,4′-Bipyridine (4,4′-bpy, 9.371 g, 60 mmol) and methyl-4-toluenesulfonate (27.00 g, 145 mmol) were added to an oven-dried 500 mL round-bottom flask fitted with a reflux condenser topped with a CaCl$_2$ guard tube. Anhydrous MeCN (350 mL) was added, then the reaction placed in a thermostated oil bath (90 °C) and stirred 12 hrs. The pale-yellow reaction

suspension was then cooled to rt., and the precipitated pale-yellow solid isolated by suction filtration (Por. 3 frit), rinsing the reaction flask with additional MeCN (2 × 50 mL). The product was washed on the frit with acetone (2 × 200 mL) then $Et_2O$ (100 mL), then dried in vacuo over $P_2O_5$, yielding the title compound as a pale-yellow powder (26.6 g, 83.9%). $^1$H-NMR (400 MHz, $D_2O$): $\delta_H$ 8.98 (d, $J_{AB}$ = 6.7 Hz, 4H, Py$^+$-**H**2,2′,6,6′), 8.42 (d, $J_{AB}$ = 6.7 Hz, 4H, Py$^+$-**H**3,3′,5,5′), 7.61 (d, $J_{AB}$ = 8.1 Hz, 4H, Ar-**H**2,6), 7.30 (d, $J_{AB}$ = 8.1 Hz, 4H, Ar-**H**3,5), 4.46 (s, 6H, N$^+$–C**H**$_3$), 2.35 (s, 6H, Ar–C**H**$_3$). FT–IR (KBr, cm$^{-1}$): 3443 (br m), 3052 (m), 1642 (m), 1567 (w), 1511 (w), 1452 (w), 1358 (w), 1177 (s), 1119 (s), 1030 (m), 1006 (m), 835 (m), 820 (m), 683 (s), 567 (s), 474 (w).

## Additional Details of Crystal Structure Refinement

### (MeV)[Mn(Clan)$_2$] (1$_{Mn}$) and (MeV)[Cd(Clan)$_2$] (1$_{Cd}$)

Crystallographic data were measured at 100 K (1$_{Mn}$) or 120 K (1$_{Cd}$) using a Rigaku XtaLAB Synergy-S diffractometer (Table S1). For both 1$_{Mn}$ and 1$_{Cd}$, data beyond $d$ = 0.8 Å were excluded from the refinement using the SHEL instructions. In 1$_{Mn}$, rigid bond restraints were applied to non-hydrogen atoms (excluding Mn) in the structure using the RIGU instruction.

### (MeV)[Mn$_2$(Clan)$_3$]·6MeCN (2a)

Crystallographic data for 2a were measured at 100 K (Table S5) using a Rigaku XtaLAB Synergy-S diffractometer. Rigid bond restraints were applied to all non-hydrogen atoms (excluding Mn) in the structure using the RIGU instruction.

### (MeV)[Mn$_2$(Fan)$_3$(H$_2$O)$_2$]·2MeCN·0.5H$_2$O (3$_{Mn}$) & (MeV)[Cd$_2$(Fan)$_3$(H$_2$O)$_2$]·2MeCN·0.6H$_2$O (3$_{Cd}$)

Crystallographic data for 3$_{Mn}$ and 3$_{Cd}$ were measured at 100 K using Rigaku XtaLAB Synergy-S diffractometer (Table S6). For both 3$_{Mn}$ and 3$_{Cd}$, rigid bond restraints were applied to all non-hydrogen atoms in the MeV$^{2+}$ cations using the RIGU instruction; in 3$_{Cd}$, similar distance restraints were also applied to all non-hydrogen atoms of the MeV$^{2+}$ cations using the SIMU instruction. For the coordinated H$_2$O molecules in 3$_{Mn}$ and 3$_{Cd}$, the H atom positions were determined by examining the $F_C-F_O$ map, with interatomic distance restraints of 0.84 Å (O–H 1,2 distance) and 1.34 Å (H···H 1,3 distance) applied using the DFIX instruction.

In 3$_{Mn}$, rigid bond and similar distance restraints were applied to the well-ordered MeCN molecule contained in the network void formed by the Mn$_4$ parallelogram, using the RIGU and SIMU instructions. Modelling of the remaining solvent was attempted, but the disorder was too severe to give a satisfactory solvent model. The scattering contribution of this disordered solvent was therefore accounted for using the SQUEEZE[4] routine of PLATON.[5] The content of disordered solvent in the compound was estimated from the electron count estimated by SQUEEZE as one MeCN and 0.5 H$_2$O per formula unit. The total estimated solvation is therefore (MeV)[Mn$_2$(Fan)$_3$(H$_2$O)$_2$]·(1+1)MeCN·0.5H$_2$O i.e. (MeV)[Mn$_2$(Fan)$_3$(H$_2$O)$_2$]·2MeCN·0.5H$_2$O. The slight discrepancy between solvation estimated by SC-XRD and that calculated by TGA and elemental analysis is due to partial solvent loss upon isolation of 3$_{Mn}$.

In 3$_{Cd}$, additional restraints were necessary for the solvent model. The thermal ellipsoids the MeCN molecule residing in the network void formed by the Cd$_4$ parallelogram, were unacceptably large when modelled at a single position. This solvent was therefore modelled as disordered over two positions, with the total occupancy fixed at one, and the occupancy of each site allowed to refine against each other. The thermal displacement parameters of equivalent atoms at the two positions were constrained to be equal using the EADP instruction. Rigid bond and similar distance restraints were applied to all non-hydrogen atoms in MeCN using the RIGU and SIMU instructions. Additional interatomic distance restraints of 1.137 Å (C≡N 1,2 distance), 1.456 Å (C–CH$_3$ 1,2 distance) and 2.593 Å (N···CH$_3$ 1,3 distance) were applied using the DFIX instruction for all MeCN molecules. Modelling of the remaining residual electron density attributed to solvent was attempted, but the disorder was too severe to give a satisfactory structure refinement. The scattering contribution of the disordered solvent was

therefore accounted for using the SQUEEZE[4] routine of PLATON.[5] The content of disordered solvent in the compound was estimated from the electron count estimated by SQUEEZE as one MeCN and 0.6 $H_2O$ per formula unit. The total estimated solvation is therefore $(MeV)[Cd_2(Fan)_3(H_2O)_2]\cdot(1+1)MeCN\cdot0.6H_2O$ i.e. $(MeV)[Cd_2(Fan)_3(H_2O)_2]\cdot2MeCN\cdot0.6H_2O$.

## [Cd(Fan)(H₂O)₂] (4Cd)

Crystallographic data for **4Cd** were collected at 100 K using the MX2 beamline of the Australian Synchrotron at $\lambda = 0.71073$ Å (Table S6), achieved using a single $\varphi$ scan ($\varphi = 0$–$360°$, $\kappa = 0°$, $\omega = 0°$), with frames collected every $0.1°$ in $\varphi$.[6] Unit cell indexing and refinement, data reduction and absorption corrections were performed using XDS.[7] For the coordinated $H_2O$ molecules, the H atom positions were determined by examining the $F_C - F_O$ map with interatomic distance restraints of 0.84 Å (O–H 1,2 distance) and 1.34 Å (H···H 1,3 distance) applied using the DFIX instruction. The data completeness to $\theta$ is low (87.6%) due to the low triclinic symmetry of **4Cd** and because the MX2 beamline only allows crystal rotation about one axis ($\varphi$).

**Table S1.** Crystallographic data for the 3D **dia** networks **1Mn** and **1Cd**.

| Compound | (MeV)[Mn(Clan)$_2$] (**1Mn**) | (MeV)[Cd(Clan)$_2$] (**1Cd**) |
|---|---|---|
| Empirical formula | C$_{24}$H$_{14}$N$_2$O$_8$Cl$_4$Mn | C$_{24}$H$_{14}$N$_2$O$_8$Cl$_4$Cd |
| Formula weight | 655.11 | 712.57 |
| Habit | Octahedron | Irregular |
| $T$ / K | 99.9(4) | 121(2) |
| Crystal system | Orthorhombic | Orthorhomic |
| Space group | *Fddd* | *Fddd* |
| $a$ / Å | 10.06100(10) | 10.0460(2) |
| $b$ / Å | 18.0409(2) | 18.1043(2) |
| $c$ / Å | 26.2770(3) | 26.7761(4) |
| $\alpha$ / ° | 90 | 90 |
| $\beta$ / ° | 90 | 90 |
| $\gamma$ / ° | 90 | 90 |
| $V$ / Å$^3$ | 4769.53(9) | 4869.92(13) |
| $Z$ | 8 | 8 |
| $\rho_{calc}$ / g cm$^{-3}$ | 1.825 | 1.944 |
| $\mu$ / mm$^{-1}$ | 9.142 | 11.730 |
| $F_{000}$ | 2632.0 | 2816.0 |
| Crystal size / mm$^3$ | 0.269 × 0.202 × 0.056 | 0.159 × 0.07 × 0.054 |
| Radiation | Cu K$\alpha$ ($\lambda$ = 1.54184 Å) | Cu K$\alpha$ ($\lambda$ = 1.54184 Å) |
| $2\theta$ range / ° | 10.616 to 149.004 | 10.6 to 148.808 |
| Index ranges | $-12 \leq h \leq 11$ $-22 \leq k \leq 19$ $-32 \leq l \leq 17$ | $-12 \leq h \leq 12$ $-22 \leq k \leq 16$ $-32 \leq l \leq 33$ |
| Total/independent reflections | 5125/1210 [$R_{int}$ = 0.0268, $R_{sigma}$ = 0.0164] | 6587/1242 [$R_{int}$ = 0.0307, $R_{sigma}$ = 0.0189] |
| Data/restraints/ parameters | 1210/48/92 | 1242/0/92 |
| Goodness-of-fit on $F^2$ | 1.083 | 1.085 |
| Final $R$ indexes [$I{\geq}2\sigma$ (*I*)] | $R_1$ = 0.0301, $wR_2$ = 0.0853 | $R_1$ = 0.0244, $wR_2$ = 0.0659 |
| Final $R$ indexes [all data] | $R_1$ = 0.0305, $wR_2$ = 0.0856 | $R_1$ = 0.0249, $wR_2$ = 0.0663 |
| Largest diff. peak/hole/ e Å$^{-3}$ | 0.35/−0.35 | 0.52/−0.58 |
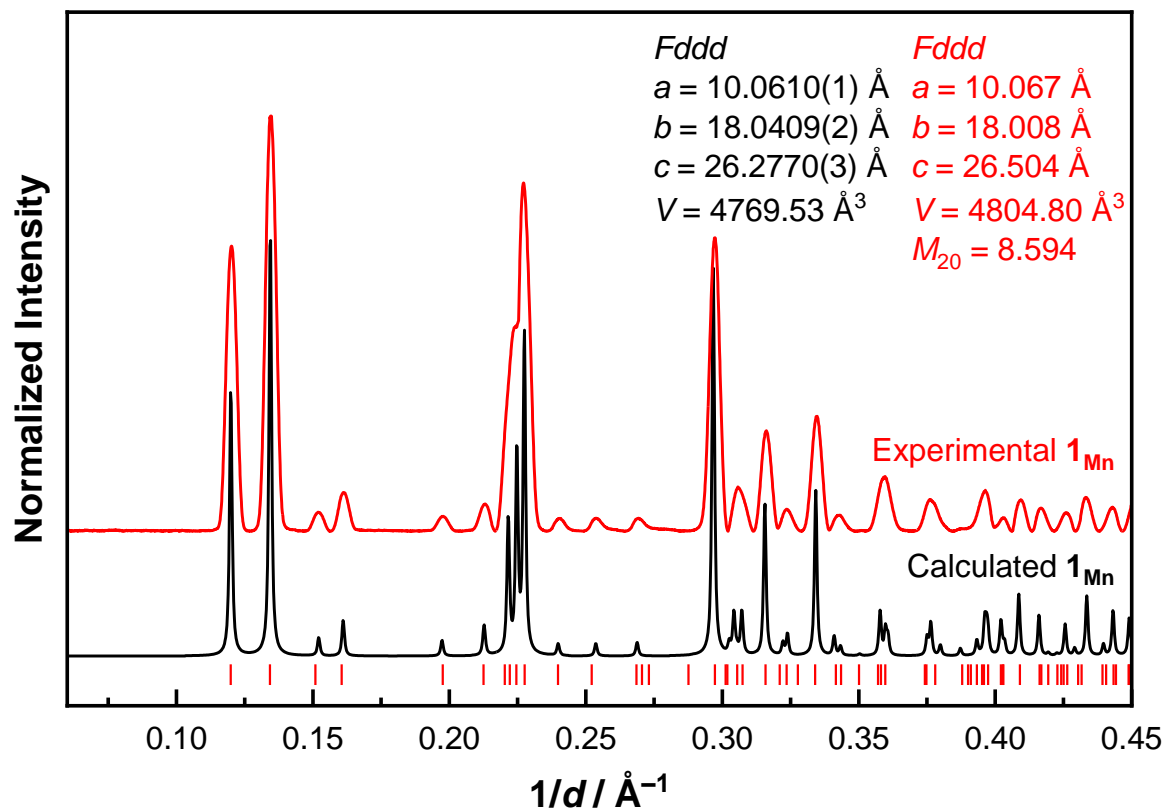
**Figure S1.** P-XRD ($\lambda = 1.54184$ Å) pattern of $\mathbf{1_{Mn}}$ (red, $T = 100$ K) and calculated pattern from SC-XRD of $\mathbf{1_{Mn}}$ (black, $T = 100$ K). Tick marks (red) indicate the positions of the allowed reflections for the unit cell indexed from the experimental P-XRD pattern.
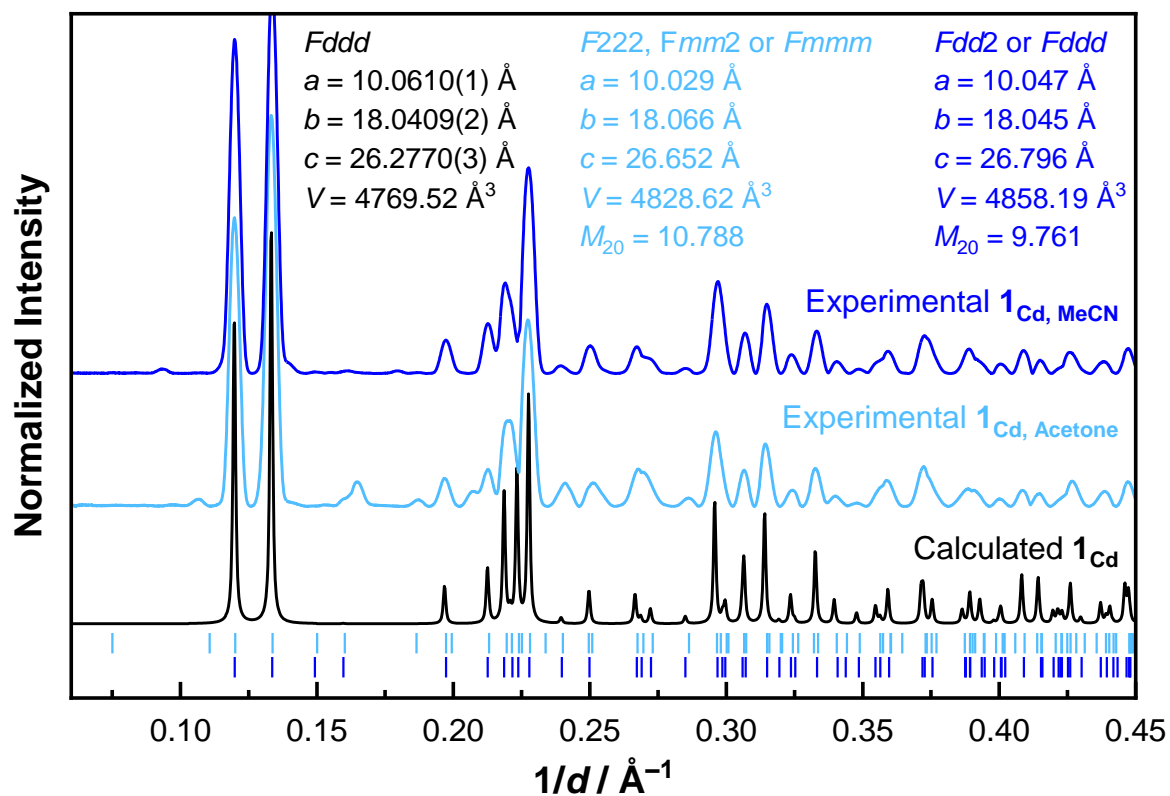
**Figure S2.** P-XRD ($\lambda$ = 1.54184 Å) pattern of **1**$_{Cd}$ synthesised using MeCN–H$_2$O (royal blue, $T$ = 100 K) or acetone–H$_2$O (pale blue, $T$ = 100 K) solvent systems, and calculated pattern from SC-XRD of **1**$_{Cd}$ (black, $T$ = 100 K). Tick marks (royal and pale blue) indicate the positions of the allowed reflections for the unit cells indexed from the experimental P-XRD patterns.
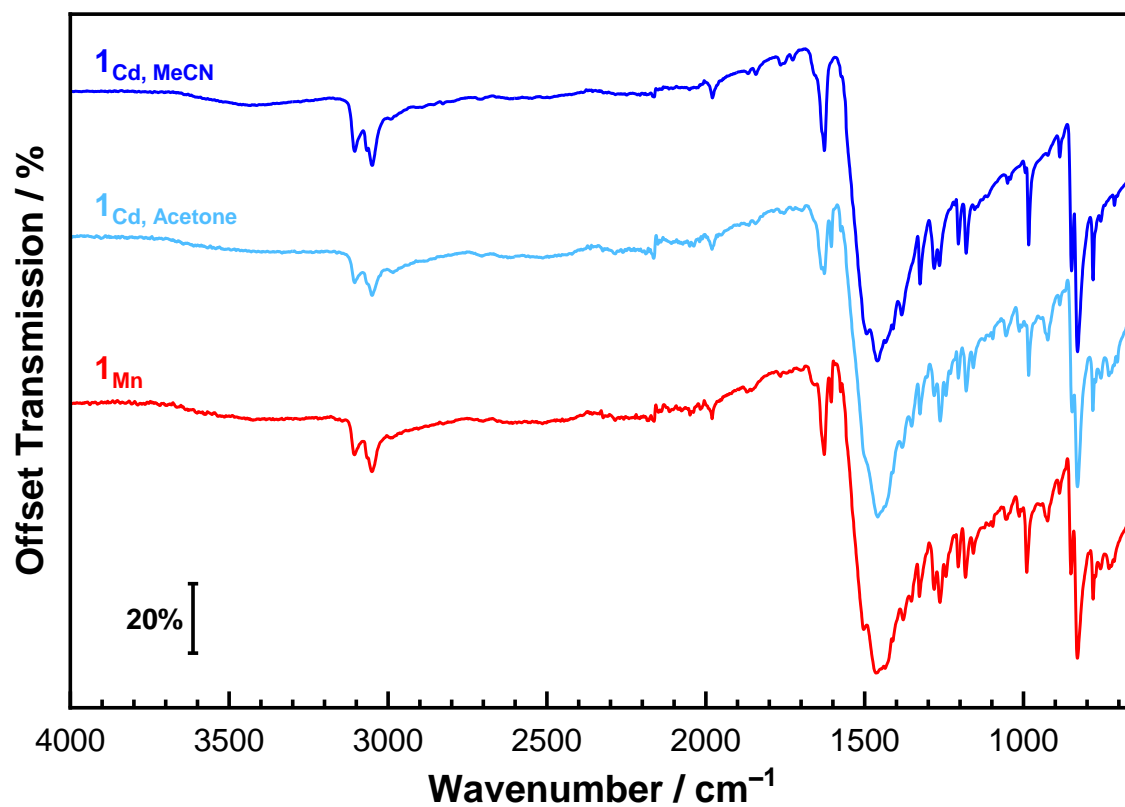
**Figure S3.** ATR FT-IR spectra of **1**$_{Mn}$ (red), and **1**$_{Cd}$ synthesised using either acetone–$H_2O$ (pale blue) or MeCN–$H_2O$ (royal blue) solvent systems, collected at room temperature in air.
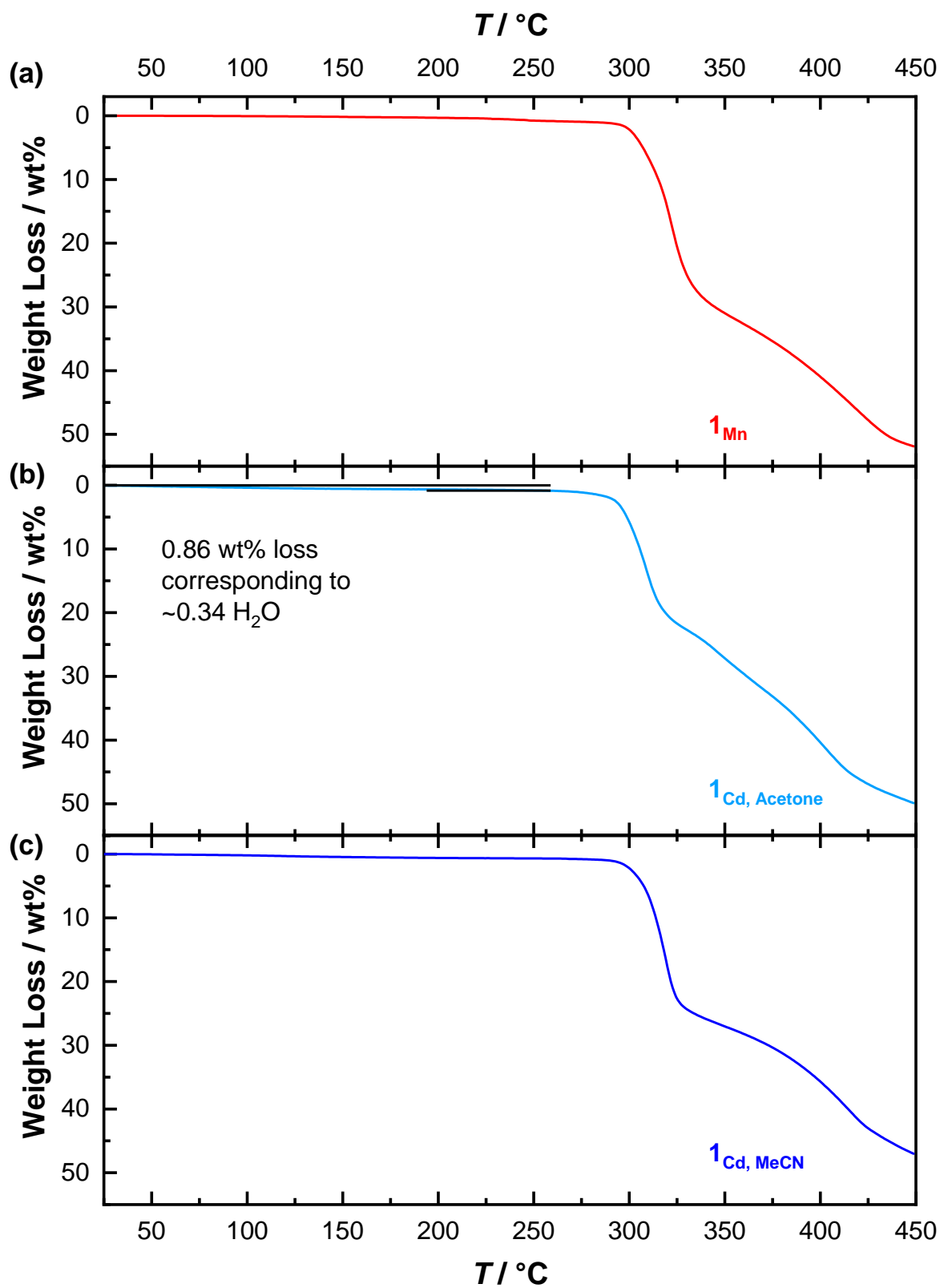
**Figure S4.** Thermogravimetric analyses of (a) **1Mn** (red), and **1Cd** synthesised using either (b) acetone–$H_2O$ (pale blue) or (c) MeCN–$H_2O$ (royal blue) solvent systems. TGA was performed at a scan rate of 5 °C min$^{-1}$ in a flow of $N_2$.

The annotation in panel (b) reads: 0.86 wt% loss corresponding to ~0.34 $H_2O$

**Table S2.** Analysis of the possible metal coordination geometries in $1_{Mn}$ and $1_{Cd}$ quantified using Continuous Shape Measure (CShM) parameters.[8, 9]

| Coordination Geometry (Symmetry) | Compound | |
|---|---|---|
| | $1_{Mn}$ | $1_{Cd}$ |
| OP-8 ($D_{8h}$) | 27.956 | 27.495 |
| HPY-8 ($C_{7v}$) | 23.647 | 23.272 |
| HBPY-8 ($D_{6h}$) | 16.730 | 16.487 |
| CU-8 ($O_h$) | 11.261 | 10.945 |
| SAPR-8 ($D_{4d}$) | 2.961 | 2.927 |
| TDD-8 ($D_{2d}$) | **0.964** | **0.801** |
| JGBF-8 ($D_{2d}$) | 12.340 | 2.922 |
| JETBPY-8 ($D_{3h}$) | 27.132 | 27.687 |
| JBTPR-8 ($C_{2v}$) | 2.349 | 2.561 |
| BTPR ($C_{2v}$) | 2.698 | 2.677 |
| JSD-8 ($D_{2d}$) | 1.153 | 1.588 |
| TT-8 ($T_d$) | 11.189 | 11.194 |

OP-8: Octagon; HPY-8: Heptagonal pyramid; HBPY-8: Heptagonal bipyramid; CU-8: Cube; SAPR-8: Square antiprism; TDD-8: Triangular dodecahedron; JGBF-8: Johnson gyrobifastigium J26; JETBPY-8: Johnson elongated triangular bipyramid J14; JBTPR-8: Biaugmented trigonal prism J50; BTPR-8: Biaugmented trigonal prism; JSD-8: Sub diphenoid J84; TT-8: Triakis tetrahedron

## Estimation of MeV$^{m+}$ Valence State

Variation of the bond lengths in viologen compounds, in particular the inter-ring C–C bond, with changes in oxidation state is well known.[10-12] The diagnostic bonds for MeV$^{m+}$ species are given in Figure S5. As aromatic MeV$^{2+}$ molecules undergo one electron reduction to the semiquinonoid MeV$^{+\bullet}$ species, followed by a subsequent one electron reduction to the neutral quinonoid MeV$^0$ form, bonds $b$ and $d$ decrease in length as they develop increasing double bond character, while bond $c$ increases in length as single bond character develops. Similarly to the methodology some of us have employed for determination of the oxidation state of TCNQ and F$_4$TCNQ in charge-transfer complexes and radical salts,[13, 14] the oxidation state of MeV$^{m+}$ species in coordination polymers can be determined by examination of particular C–C bond lengths, using an empirical relationship introduced by Kistenmacher $et$ $al.$ for TCNQ,[15]

$$q = A\left(\frac{c}{b+d}\right) + B \qquad (1)$$

where $q$ (-) is the estimated charge, $b$, $c$ and $d$ (Å) are the bond lengths shown in Figure S5, and $A$ and $B$ are empirical fitting parameters calculated from analysis of SC-XRD structures of MeV$^0$, MeV$^{+\bullet}$ and MeV$^{2+}$ species in literature (Table S3). Based upon these compounds, the $A$ and $B$ parameters were calculated to be −37.932 and 20.468 respectively.
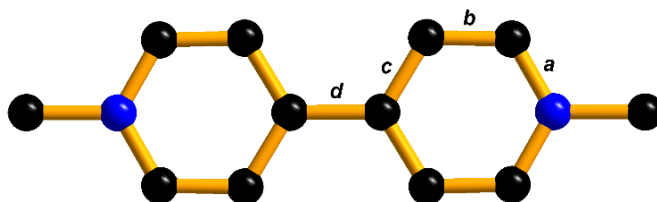


**Figure S5.** Diagnostic bond lengths in MeV$^{m+}$ species for estimation of oxidation state. Blue = N and black = C.

**Table S3.** Summary of the diagnostic mean bond lengths in MeV$^0$, MeV$^{+\bullet}$ and MeV$^{2+}$ species reported in literature for calculation of Kistenmacher relationship parameters. NB. Where multiple values for the bond lengths are shown, they represent the mean values for crystallographically unique moieties in the asymmetric unit.

| Compound | Assumed Charge ($m$) | $a$ / Å | $b$ / Å | $c$ / Å | $d$ / Å | $c/(b + d)$ | $q$ | Ref. |
|---|---|---|---|---|---|---|---|---|
| MeV$^0$ | 0 | 1.381 | 1.331 | 1.453 | 1.363 | 0.539 | 0.01 | 10 |
| | | 1.383 | 1.330 | 1.458 | 1.370 | 0.540 | -0.02 | |
| (MeV$^{+\bullet}$)PF$_6$ | 1 | 1.357 | 1.342 | 1.437 | 1.399 | 0.524 | 0.58 | 10 |
| | | 1.387 | 1.344 | 1.399 | 1.442 | 0.502 | 1.42 | |
| (MeV$^{+\bullet}$)BF$_4$ | 1 | 1.359 | 1.349 | 1.423 | 1.424 | 0.513 | 1.00 | 11 |
| | | 1.355 | 1.355 | 1.426 | 1.427 | 0.513 | 1.02 | |
| MeV$^{2+}$(PF$_6$)$_2$ | 2 | 1.328 | 1.354 | 1.383 | 1.485 | 0.487 | 1.99 | 16 |
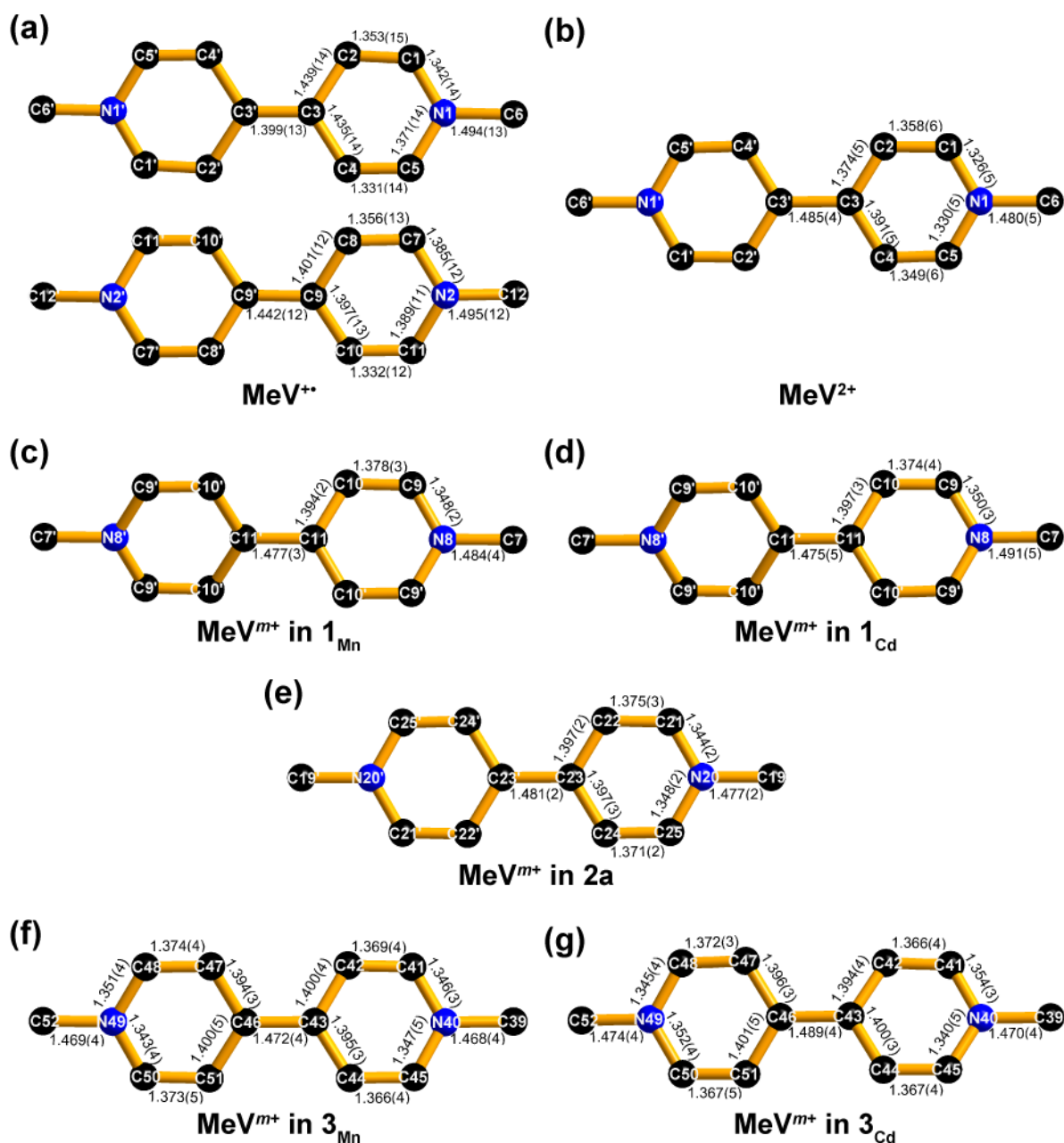
**Figure S6.** Bond lengths in MeV$^{m+}$ moieties in (a) (MeV)PF$_6$,[10] (b) MeV(PF$_6$)$_2$,[16], (c) **1$_{Mn}$**, (d) **1$_{Cd}$**, (e) **2a**, (f) **3$_{Mn}$** and (g) **3$_{Cd}$**. For (MeV)PF$_6$, the two species shown are the crystallographically independent molecules in the asymmetric unit. Blue = N and black = C. H atoms not shown for clarity.

**Table S4.** Summary of the mean diagnostic bond lengths and estimated charge ($q$) for MeV$^{m+}$ moieties in coordination polymers in this work.

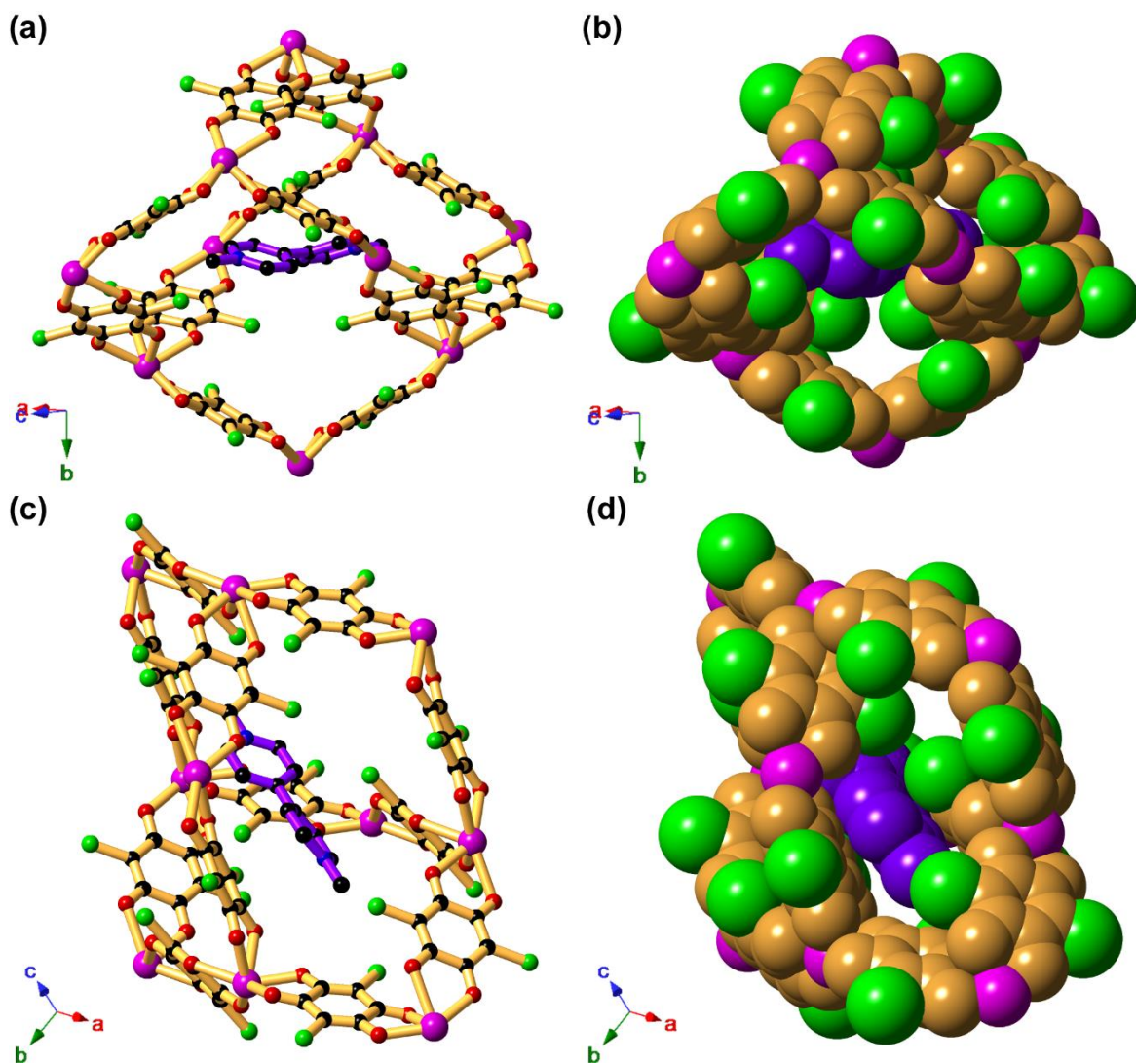| Compound | $a$ / Å | $b$ / Å | $c$ / Å | $d$ / Å | $c/(b + d)$ | $q$ |
|:---:|:---:|:---:|:---:|:---:|:---:|:---:|
| $1_{Mn}$ | 1.348 | 1.378 | 1.394 | 1.477 | 0.488 | 1.95 |
| $1_{Cd}$ | 1.350 | 1.374 | 1.397 | 1.475 | 0.490 | 1.87 |
| $2a$ | 1.346 | 1.373 | 1.397 | 1.481 | 0.489 | 1.90 |
| $3_{Mn}$ | 1.347 | 1.371 | 1.397 | 1.472 | 0.492 | 1.82 |
| $3_{Cd}$ | 1.348 | 1.368 | 1.398 | 1.489 | 0.489 | 1.91 |

**Figure S7.** Ball-and-stick (a, c) and spacefilling (b, d) representations of the interactions between MeV$^{2+}$ cations (purple) and the anionic [Mn(Clan)$_2$]$^{2-}$ adamantane unit (tan) in **1$_{Mn}$**. Magenta = Mn, green = Cl, red = O, and black = C. H atoms not shown for clarity.

**Table S5.** Crystallographic data for the 2D honeycomb network **2a**.

| Compound | $(MeV)[Mn_2(Clan)_3]\cdot 6MeCN$ (**2a**) |
|---|---|
| Empirical formula | $C_{21}H_{16}N_4O_6Cl_3Mn$ |
| Formula weight | 581.67 |
| Habit | Plate |
| $T$ / K | 100.0(5) |
| Crystal system | Triclinic |
| Space group | $P{-}1$ |
| $a$ / Å | 8.71340(10) |
| $b$ / Å | 11.69370(10) |
| $c$ / Å | 12.4715(2) |
| $\alpha$ / ° | 75.2910(10) |
| $\beta$ / ° | 78.4070(10) |
| $\gamma$ / ° | 83.1470(10) |
| $V$ / Å$^3$ | 1200.89(3) |
| $Z$ | 2 |
| $\rho_{calc}$ / g cm$^{-3}$ | 1.609 |
| $\mu$ / mm$^{-1}$ | 7.950 |
| $F_{000}$ | 588.0 |
| Crystal size / mm$^3$ | $0.267 \times 0.17 \times 0.031$ |
| Radiation | Cu K$\alpha$ ($\lambda = 1.54184$ Å) |
| $2\theta$ range / ° | 7.448 to 148.96 |
| Index ranges | $-10 \leq h \leq 10$<br>$-14 \leq k \leq 14$<br>$-15 \leq l \leq 15$ |
| Total/independent reflections | 40457/4893<br>[$R_{int} = 0.0405$,<br>$R_{sigma} = 0.0181$] |
| Data/restraints/ parameters | 4893/153/320 |
| Goodness-of-fit on $F^2$ | 1.029 |
| Final $R$ indexes [$I{\geq}2\sigma$ ($I$)] | $R_1 = 0.0253$,<br>$wR_2 = 0.0661$ |
| Final $R$ indexes [all data] | $R_1 = 0.0258$,<br>$wR_2 = 0.0664$ |
| Largest diff. peak/hole/ e Å$^{-3}$ | 0.31/−0.30 |
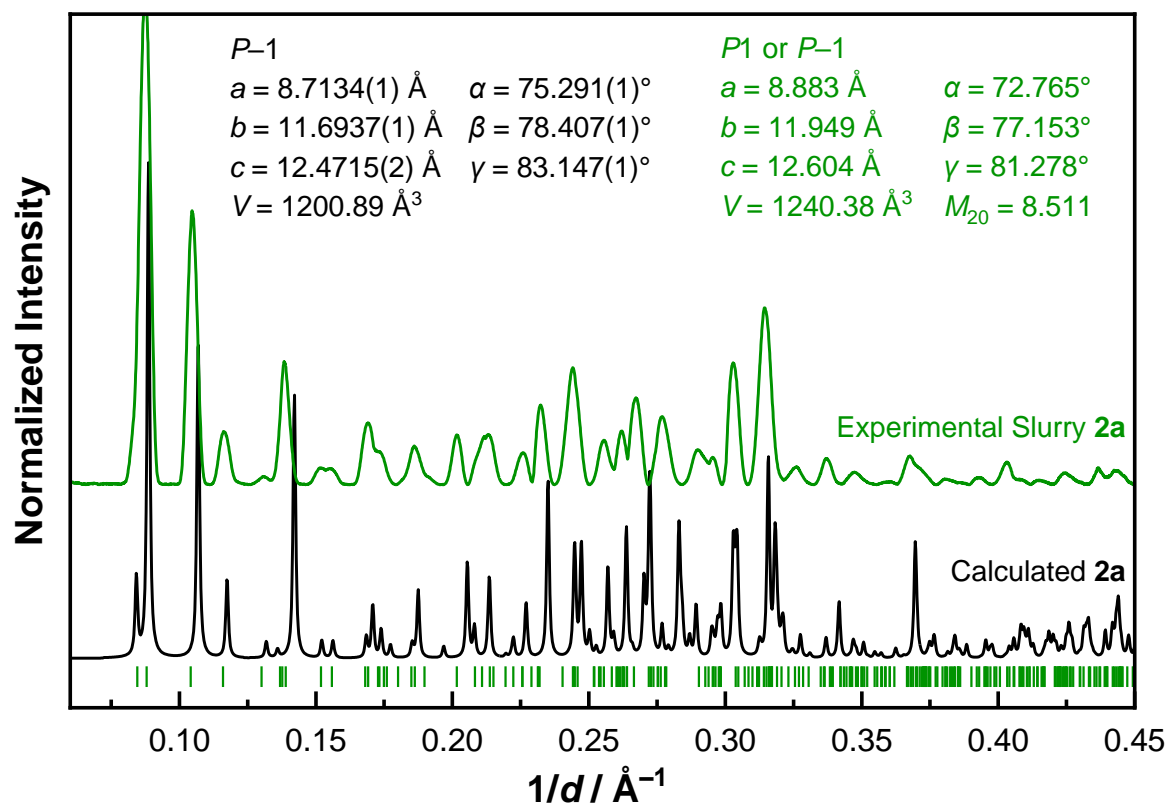
**Figure S8.** P-XRD ($\lambda$ = 1.54184 Å) pattern of a MeCN slurry of bulk **2a** (green, $T$ = 250 K) and calculated pattern from SC-XRD of **2a** (black, $T$ = 100 K). Tick marks (green) indicate the positions of the allowed reflections for the unit cell indexed from the experimental P-XRD pattern.
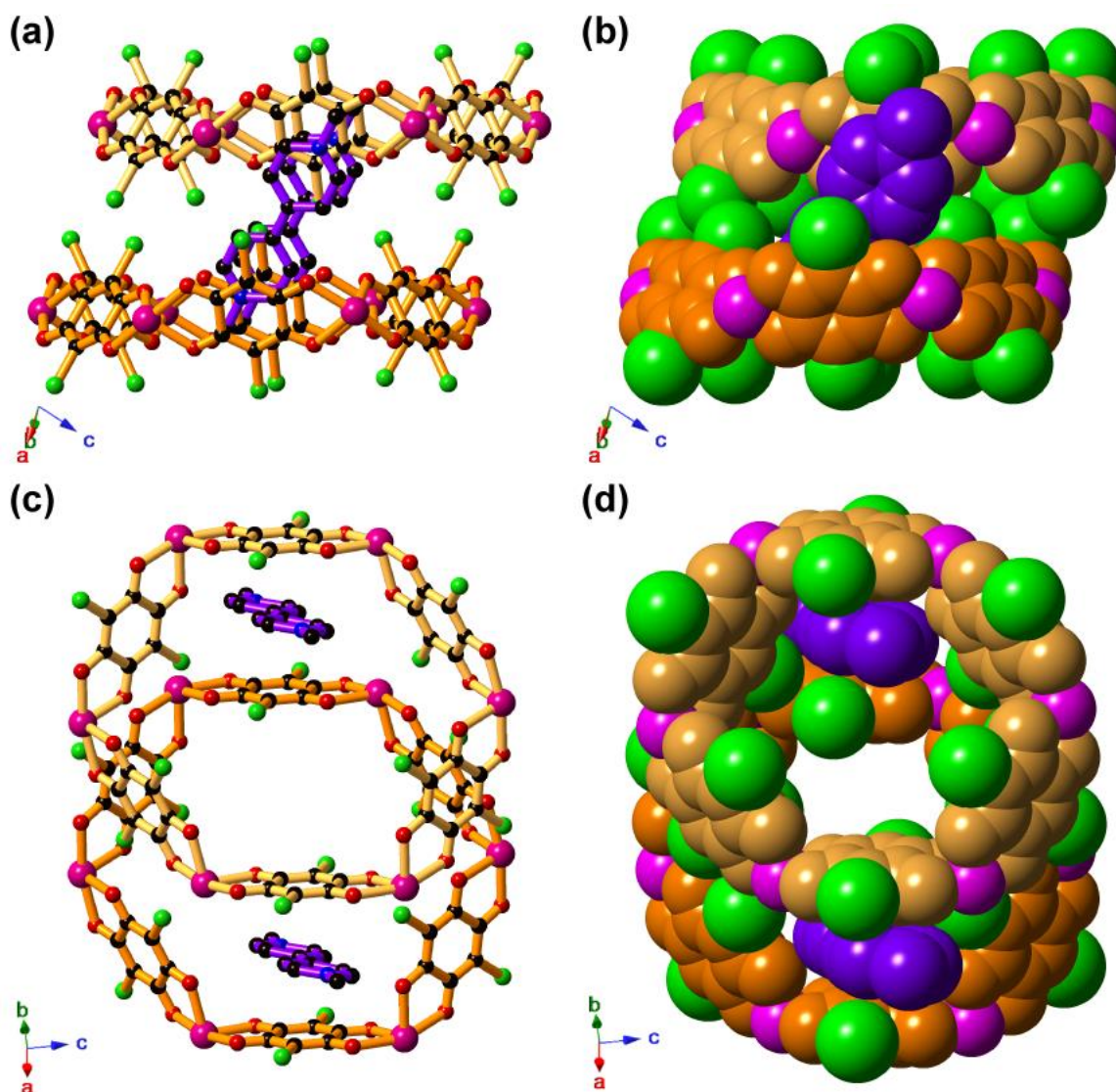
**Figure S9.** Ball-and-stick (a, c) and spacefilling (b, d) representations of the interactions between MeV$^{2+}$ cations (purple) and anionic [Mn$_2$(Clan)$_3$]$^{2-}$ sheets above (tan) and below (orange). Views along (a, b) the plane of the anionic [Mn$_2$(Clan)$_3$]$^{2-}$ sheets, and (c, d) along the one-dimensional channels. Magenta = Mn, green = Cl, red = O, blue = N, black = C. H atoms and ordered MeCN in channels not shown for clarity.
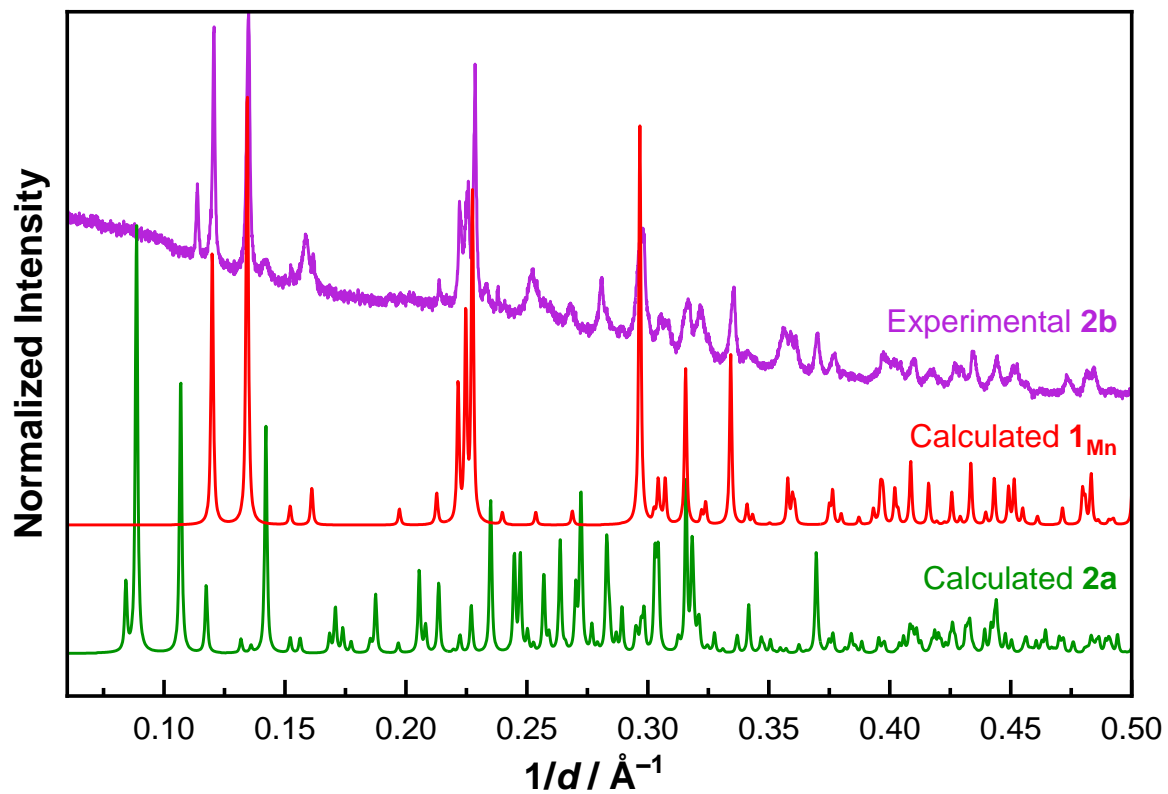
**Figure S10.** Synchrotron P-XRD ($\lambda$ = 0.58835 Å) pattern of bulk **2b** (i.e. isolated **2a**, magenta, $T$ = 100 K) and calculated patterns from SC-XRD of **1$_{Mn}$** (red, $T$ = 100 K) and **2a** (green, $T$ = 100 K).
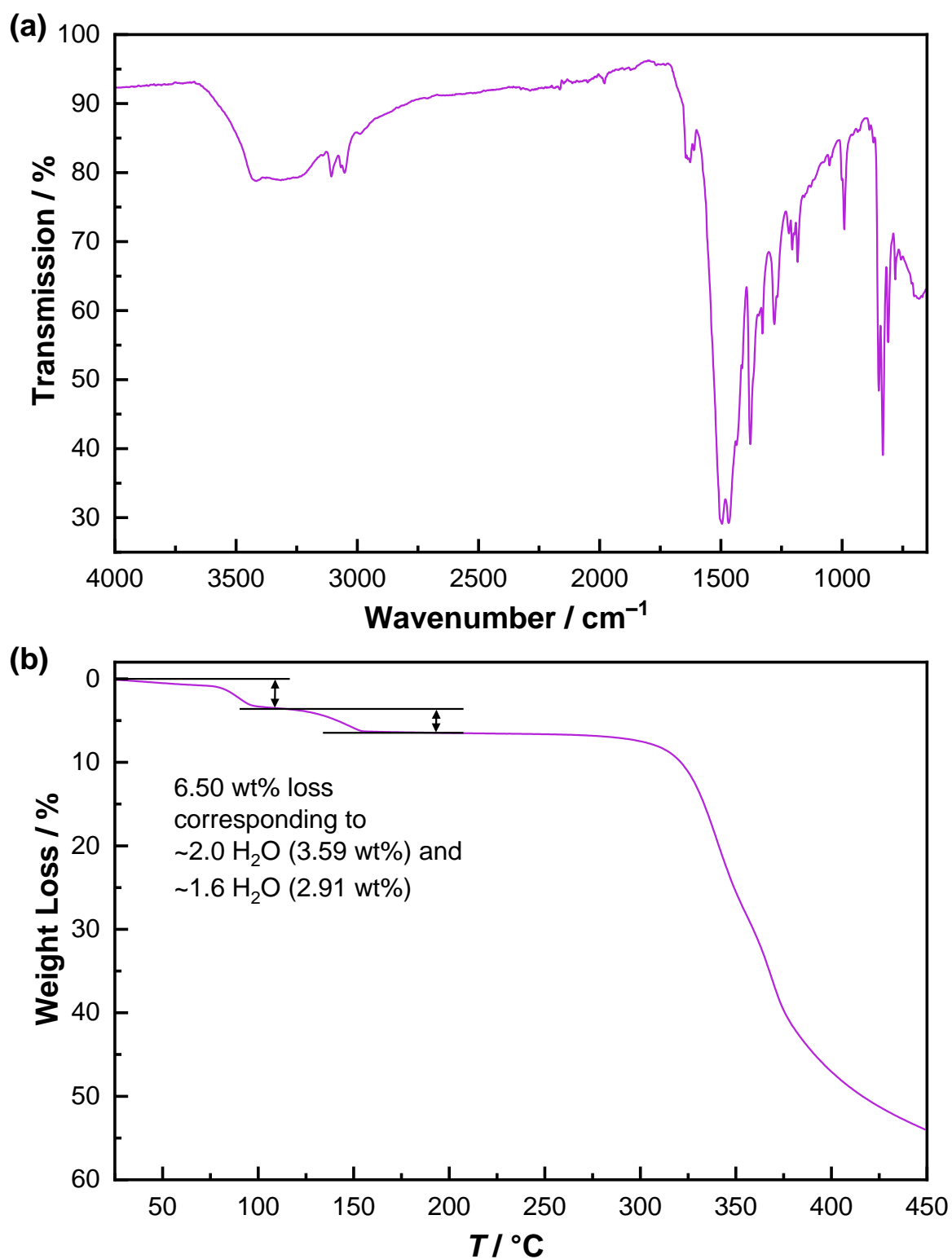
**(a)** ATR FT-IR spectrum of **2b** collected at room temperature in air. **(b)** Thermogravimetric analysis of **2b** showing two distinct mass loss processes. TGA was performed at a scan rate of 5 °C min$^{-1}$ in a flow of $N_2$.

Plot (b) labels: 6.50 wt% loss corresponding to ~2.0 $H_2O$ (3.59 wt%) and ~1.6 $H_2O$ (2.91 wt%)

**Figure S11.**

**Table S6.** Crystallographic data for the 1D coordination polymers $3_{Mn}$, $3_{Cd}$ and $4_{Cd}$.

| Compound | (MeV)[Mn₂(Fan)₃(H₂O)₂]·2MeCN·0.5H₂O ($3_{Mn}$) | (MeV)[Cd₂(Fan)₃(H₂O)₂]·2MeCN·0.6H₂O ($3_{Cd}$) | [Cd(Fan)(H₂O)₂] ($4_{Cd}$) |
|---|---|---|---|
| Empirical formula | $C_{34}H_{25}N_4O_{14.5}F_6Mn_2$[a] | $C_{34}H_{25.2}N_4O_{14.6}F_6Cd_2$[b] | $C_6H_4CdF_2O_6$ |
| Formula weight | 945.46[a] | 1062.18[b] | 322.49 |
| Habit | Plate | Plate | Plate |
| $T$ / K | 100.00(1) | 100.00(10) | 100.15 |
| Crystal system | Triclinic | Triclinic | Monoclinic |
| Space group | $P{-}1$ | $P{-}1$ | $C2/m$ |
| $a$ / Å | 11.9381(2) | 12.01850(10) | 6.6686(13) |
| $b$ / Å | 12.4271(2) | 12.37350(10) | 8.0832(16) |
| $c$ / Å | 13.8921(2) | 13.86430(10) | 8.1130(16) |
| $\alpha$ / ° | 97.9620(10) | 96.0150(10) | 90 |
| $\beta$ / ° | 114.4250(10) | 114.1410(10) | 112.03(3) |
| $\gamma$ / ° | 95.4990(10) | 95.2320(10) | 90 |
| $V$ / Å³ | 1831.45(5) | 1850.57(3) | 405.40(16) |
| $Z$ | 2 | 2 | 2 |
| $\rho_{calc}$ / g cm⁻³ | 1.714 | 1.906 | 2.642 |
| $\mu$ / mm⁻¹ | 6.592 | 10.180 | 2.738 |
| $F_{000}$ | 954.0[a] | 1048.0[b] | 308.0 |
| Crystal size / mm³ | 0.194 × 0.085 × 0.022 | 0.252 × 0.14 × 0.035 | 0.05 × 0.05 × 0.01 |
| Radiation | Cu K$\alpha$ ($\lambda$ = 1.54184 Å) | Cu K$\alpha$ ($\lambda$ = 1.54184 Å) | Synchrotron ($\lambda$ = 0.71073 Å) |
| $2\theta$ range / ° | 7.128 to 155.914 | 7.074 to 156.264 | 5.416 to 63.014 |
| Index ranges | $-15 \le h \le 14$ $-15 \le k \le 15$ $-15 \le l \le 17$ | $-14 \le h \le 15$ $-15 \le k \le 15$ $-17 \le l \le 17$ | $-9 \le h \le 9$ $-11 \le k \le 11$ $-10 \le l \le 10$ |
| Total/independent reflections | 28688/7660 [$R_{int}$ = 0.0390, $R_{sigma}$ = 0.0368] | 28800/7747 [$R_{int}$ = 0.0340, $R_{sigma}$ = 0.0296] | 3614/629 [$R_{int}$ = 0.0622, $R_{sigma}$ = 0.0312] |
| Data/restraints/parameters | 7660/132/533 | 7747/252/544 | 629/2/43 |
| Goodness-of-fit on $F^2$ | 1.038 | 1.080 | 1.149 |
| Final $R$ indexes [$I \ge 2\sigma(I)$] | $R_1$ = 0.0359, $wR_2$ = 0.0977 | $R_1$ = 0.0251, $wR_2$ = 0.0674 | $R_1$ = 0.0306, $wR_2$ = 0.0809 |
| Final $R$ indexes [all data] | $R_1$ = 0.0437, $wR_2$ = 0.1039 | $R_1$ = 0.0270, $wR_2$ = 0.0686 | $R_1$ = 0.306, $wR_2$ = 0.089 |
| Largest diff. peak/hole/ e Å⁻³ | 0.35/−0.44 | 0.44/−0.84 | 2.02/−1.41 |

Includes contribution of [a]: one MeCN and 0.5 H₂O ($3_{Mn}$); [b]: and one MeCN and 0.6 H₂O ($3_{Cd}$) disordered molecules per formula unit. The scattering contribution was accounted using the SQUEEZE[4] routine in PLATON.[5]
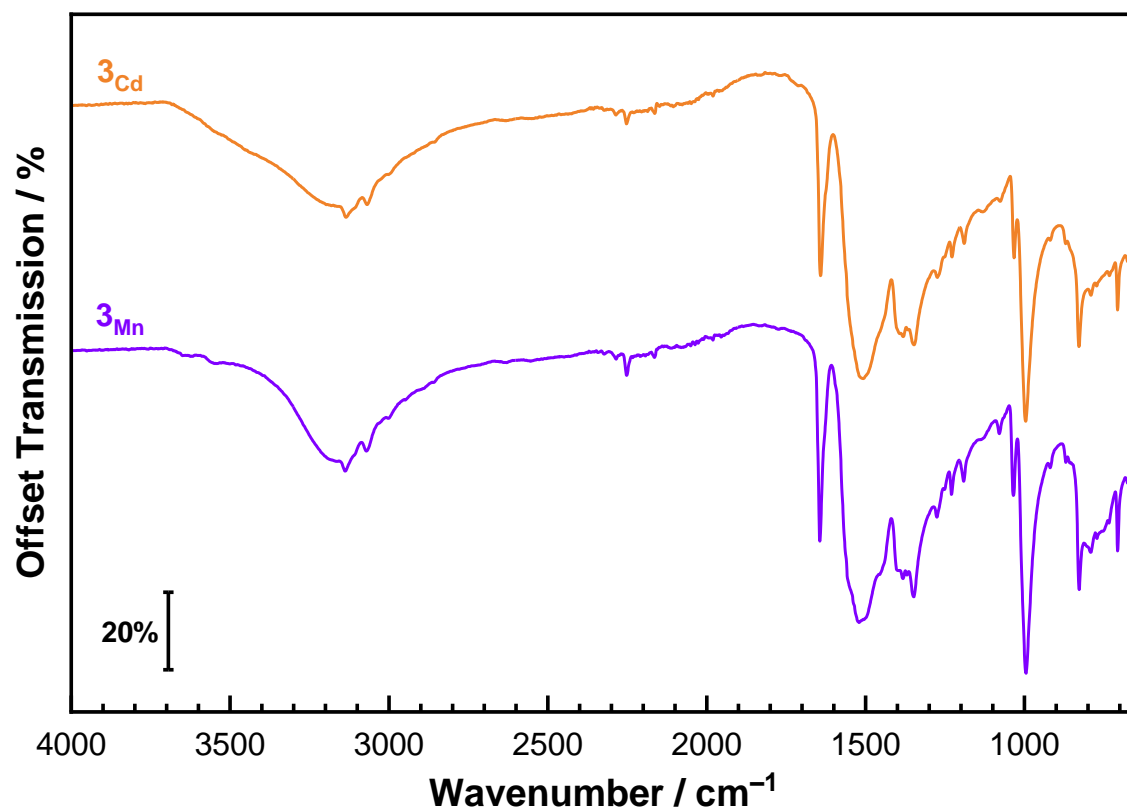
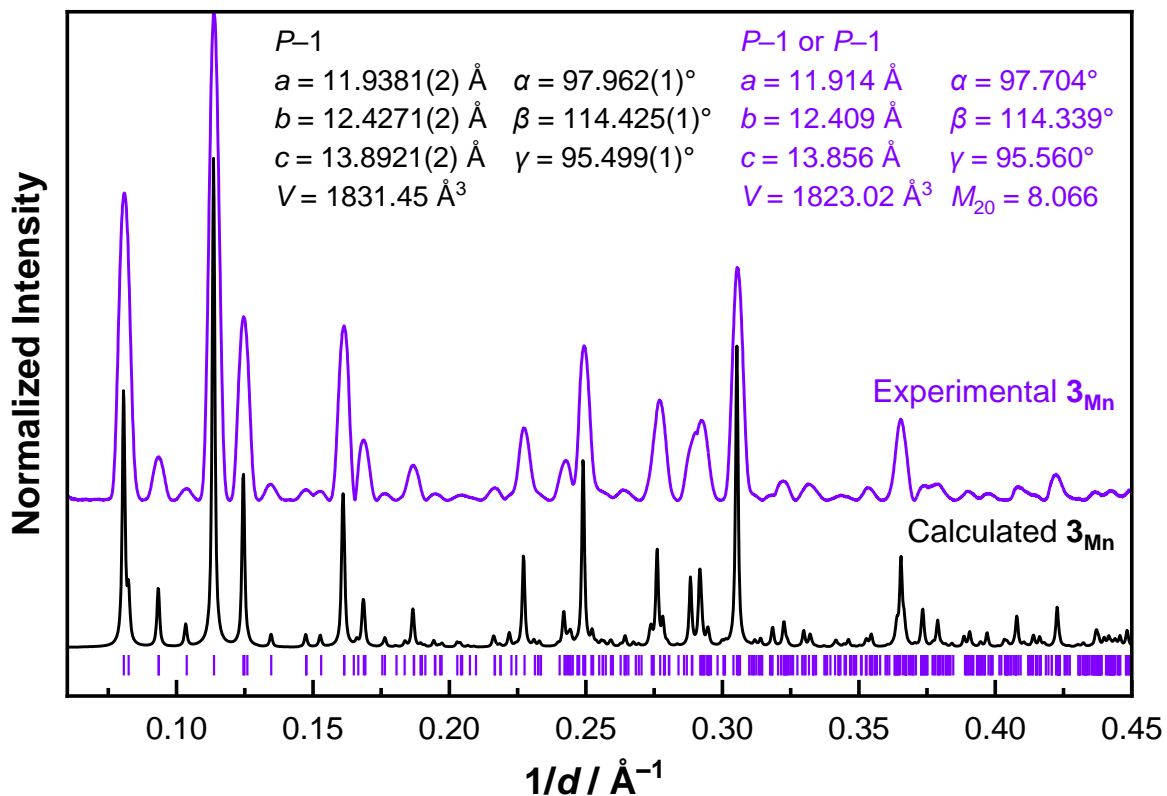**Figure S12.** ATR FT-IR spectra of **3**Mn (purple) and **3**Cd (orange) collected at room temperature in air.

**Figure S13.** P-XRD ($\lambda = 1.54184$ Å) pattern of **3$_{Mn}$** (purple, $T = 100$ K) and calculated pattern from SC-XRD of **3$_{Mn}$** (black, $T = 100$ K). Tick marks (purple) indicate the positions of the allowed reflections for the unit cell indexed from the experimental P-XRD pattern.
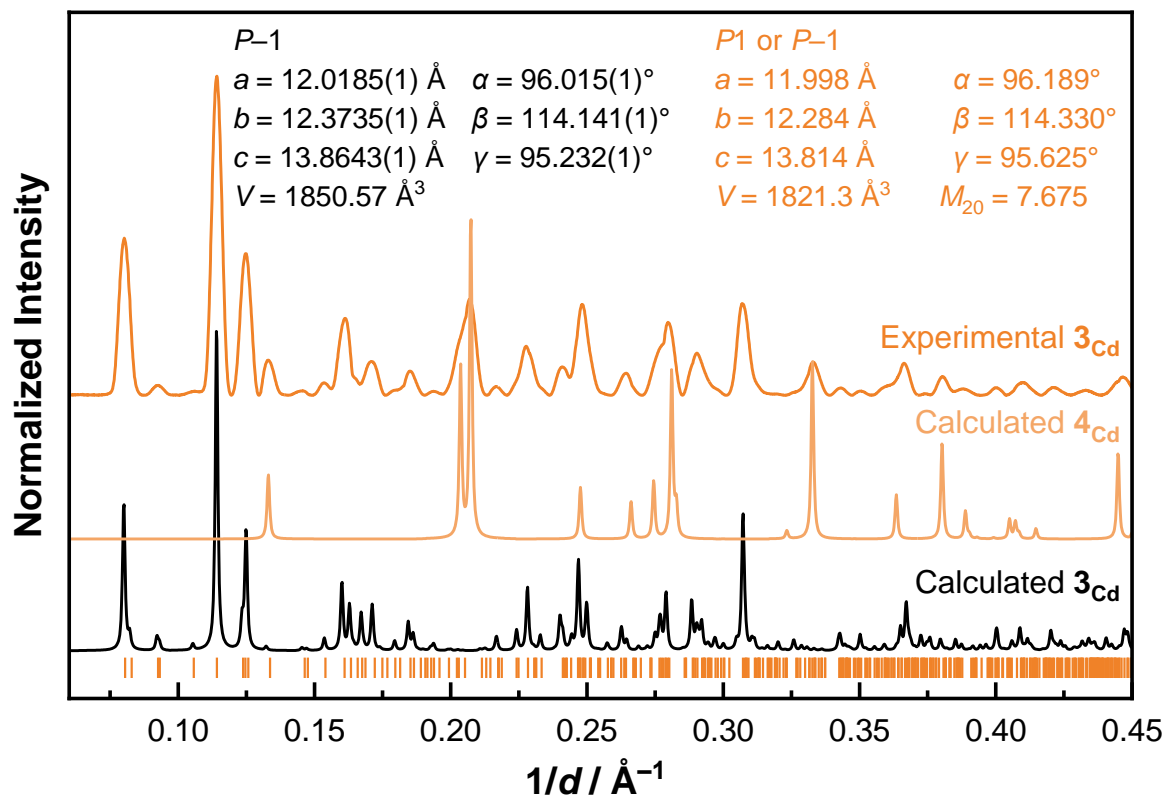
**Figure S14.** P-XRD ($\lambda$ = 1.54184 Å) pattern of bulk **3$_{Cd}$** (dark orange, $T$ = 100 K) and calculated patterns from SC-XRD of **3$_{Cd}$** (black, $T$ = 100 K) and **4$_{Cd}$** (light orange, $T$ = 100 K). Tick marks (dark orange) indicate the positions of the allowed reflections for the state unit cell indexed from the experimental P-XRD pattern. NB: Peaks in the experimental P-XRD attributed to the **4$_{Cd}$** phase have been excluded from the pattern indexing.

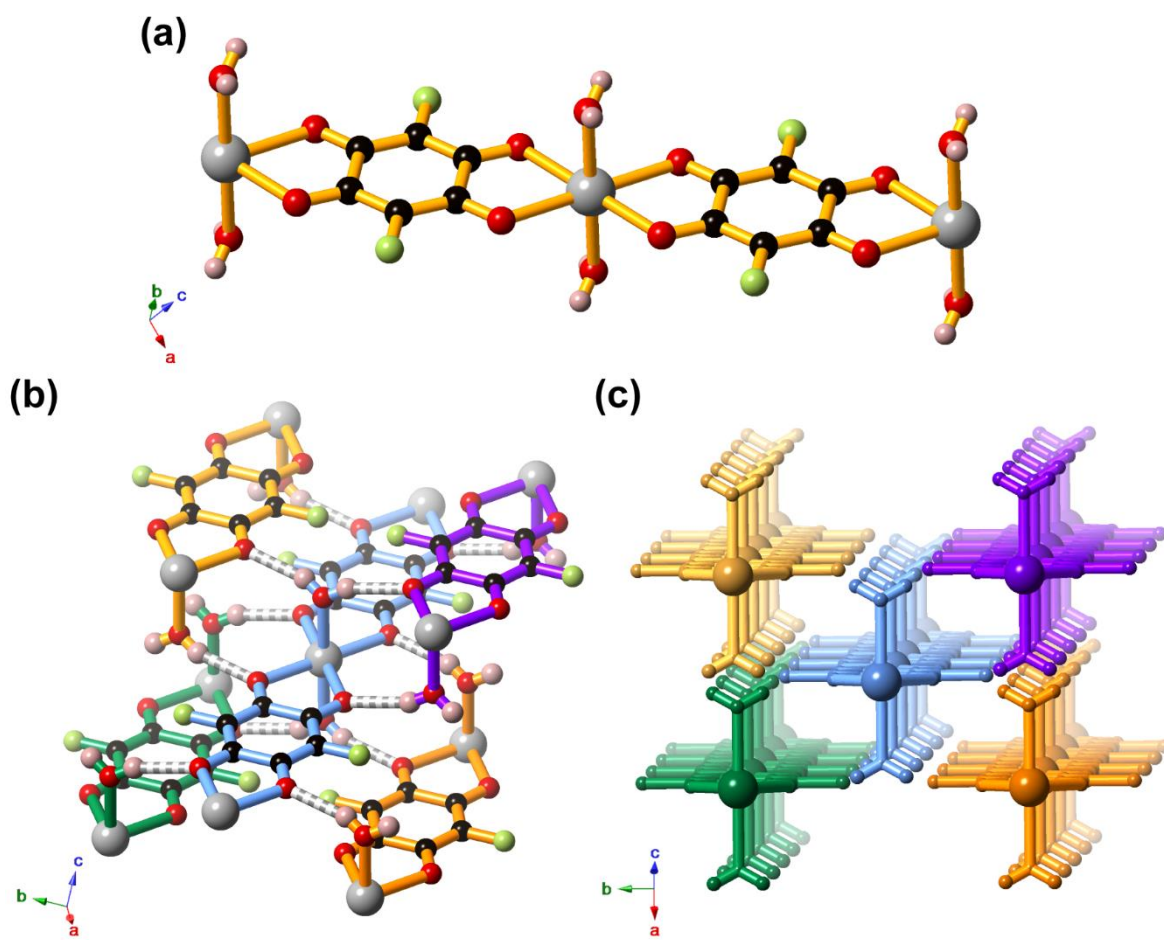**Figure S15.** The structure of $[Cd(Fan)(H_2O)_2]$ (**4**$_{Cd}$) 1D strip coordination polymer. (a) Coordination environment around $Cd^{II}$ centres in **4**$_{Cd}$. (b) H-bonding interactions betweens each coordinated $H_2O$ molecule and adjacent $[Cd(Fan)(H_2O)_2]$ strips in **4**$_{Cd}$. (c) Packing arrangement of $[Cd(Fan)(H_2O)_2]$ with adjacent 1D strips in **4**$_{Cd}$.

**Table S7.** Atomic separations and angles involving selected close contacts between C–H units of MeV$^{2+}$ cations with Clan$^{2-}$ and Fan$^{2-}$ ligands within **1$_{Mn}$**, **1$_{Cd}$**, **2a**, **3$_{Mn}$** and **3$_{Cd}$**.

| Compound | Atoms | H···X / Å | C–H···X / Å | C–H···X / ° |
|---|---|---|---|---|
| **1$_{Mn}$** | C10–H10···O1$^{I}$ | 2.51 | 3.44 | 166.6 |
| | C10–H10···O5 | 2.56 | 3.19 | 124.7 |
| **1$_{Cd}$** | C10–H10···O1$^{II}$ | 2.53 | 3.46 | 164.9 |
| | C10–H10···O5$^{III}$ | 2.56 | 3.20 | 124.6 |
| **2a** | C22–H22···O13$^{IV}$ | 2.38 | 3.32 | 170.4 |
| | C24–H24···O13$^{V}$ | 2.41 | 3.34 | 166.1 |
| **3$_{Mn}$** | C50–H50···O1$^{VI}$ | 2.27 | 3.13 | 150.0 |
| | C45–H45···O36$^{VI}$ | 2.44 | 2.99 | 116.5 |
| | C42–H42···O15$^{VII}$ | 2.49 | 3.41 | 164.1 |
| | C48–H48···F18$^{VII}$ | 2.29 | 2.91 | 157.4 |
| **3$_{Cd}$** | C50–H50···O1$^{VI}$ | 2.27 | 3.11 | 148.0 |
| | C45–H45···O36$^{VI}$ | 2.43 | 3.04 | 121.3 |
| | C42–H42···O15$^{VII}$ | 2.44 | 3.37 | 166.2 |
| | C48–H48···F18$^{VII}$ | 2.29 | 2.92 | 123.0 |

[I] 0.25 + $x$, 1-$y$, 0.25+$z$; [II] $x$, 1.25-$y$, 1.25-$z$; [III] 0.25+$x$, 0.25+$y$, 1-$z$; [IV] +$x$, 1+$y$, +$z$; [V] 2-$x$, 1-$y$, -$z$; [VI] 1-$x$, -$y$, -$z$; [VII] 1-$x$, 1-$y$, 1-$z$. X = O or F.

# References

(1)     Wallenfels, K.; Friedrich, K., Über Fluorchinone, II. Zur Hydrolyse Und Alkoholyse Des Fluoranils. *Chem. Ber.* **1960,** 93, (12), 3070-3082.

(2)     Essers, M.; Haufe, G., Chemical Consequences of Fluorine Substitution. Part 4. Diels–Alder Reactions of Fluorinated *p*-Benzoquinones with Dane's Diene. Synthesis of Fluorinated D-Homosteroids. *J. Chem. Soc., Perkin Trans. 1* **2002**, (23), 2719-2728.

(3)     Kingsbury, C. J.; Abrahams, B. F.; D'Alessandro, D. M.; Hudson, T. A.; Murase, R.; Robson, R.; White, K. F., Role of $NEt_4^+$ in Orienting and Locking Together $[M_2lig_3]^{2-}$ (6,3) Sheets ($H_2lig$ = Chloranilic or Fluoranilic Acid) to Generate Spacious Channels Perpendicular to the Sheets. *Cryst. Growth Des.* **2017,** 17, (4), 1465-1470.

(4)     Spek, A. L., PLATON SQUEEZE: A Tool for the Calculation of the Disordered Solvent Contribution to the Calculated Structure Factors. *Acta Crystallogr. C* **2015,** 71, (1), 9-18.

(5)     Spek, A. L., Structure Validation in Chemical Crystallography. *Acta Crystallogr. D* **2009,** 65, (2), 148-155.

(6)     Aragao, D.; Aishima, J.; Cherukuvada, H.; Clarken, R.; Clift, M.; Cowieson, N. P.; Ericsson, D. J.; Gee, C. L.; Macedo, S.; Mudie, N.; Panjikar, S.; Price, J. R.; Riboldi-Tunnicliffe, A.; Rostan, R.; Williamson, R.; Caradoc-Davies, T. T., MX2: A High-Flux Undulator Microfocus Beamline Serving Both the Chemical and Macromolecular Crystallography Communities at the Australian Synchrotron. *J. Synchrotron Rad.* **2018,** 25, (3), 885-891.

(7)     Kabsch, W., XDS. *Acta Crystallogr. D* **2010,** 66, (2), 125-132.

(8)     Alvarez, S., Distortion Pathways of Transition Metal Coordination Polyhedra Induced by Chelating Topology. *Chem. Rev.* **2015,** 115, (24), 13447-13483.

(9)     Llunell, M.; Casanova, D.; Cicera, J.; Alemany, P.; Alvarez, S., *SHAPE, Version 2.1.* ed.; Universitat de Barcelona: Barcelona, Spain, 2013.

(10)    Bockman, T. M.; Kochi, J. K., Isolation and Oxidation-Reduction of Methylviologen Cation Radicals. Novel Disproportionation in Charge-Transfer Salts by X-ray Crystallography. *J. Org. Chem.* **1990,** 55, (13), 4127-4135.

(11)    Leblanc, N.; Mercier, N.; Toma, O.; Kassiba, A. H.; Zorina, L.; Auban-Senzier, P.; Pasquier, C., Unprecedented Stacking of $MV^{2+}$ Dications and $MV^{\bullet+}$ Radical Cations in the Mixed-Valence Viologen Salt $(MV)_2(BF_4)_3$ (MV = Methylviologen). *Chem. Commun.* **2013,** 49, (87), 10272-10274.

(12)    Porter, W. W., III; Vaid, T. P., Isolation and Characterization of Phenyl Viologen as a Radical Cation and Neutral Molecule. *J. Org. Chem.* **2005,** 70, (13), 5028-5035.

(13)    Sutton, A. L.; Abrahams, B. F.; D'Alessandro, D. M.; Elliott, R. W.; Hudson, T. A.; Robson, R.; Usov, P. M., Structural and Optical Investigations of Charge Transfer Complexes Involving the $F_4TCNQ$ Dianion. *CrystEngComm* **2014,** 16, (24), 5234-5243.

(14)    Sutton, A. L.; Abrahams, B. F.; D'Alessandro, D. M.; Hudson, T. A.; Robson, R.; Usov, P. M., Structural and Optical Investigations of Charge Transfer Complexes Involving the Radical Anions of TCNQ and $F_4TCNQ$. *CrystEngComm* **2016,** 18, (46), 8906-8914.

(15)    Kistenmacher, T. J.; Emge, T. J.; Bloch, A. N.; Cowan, D. O., Structure of the Red, Semiconducting Form of 4,4',5,5'-Tetramethyl-$\Delta^{2,2'}$-bi-1,3-diselenole-7,7,8,8-tetracyano-*p*-quinodimethane, TMTSF–TCNQ. *Acta Crystallogr. B* **1982,** 38, (4), 1193-1199.

(16)    Huang, F.; Switek, K. A.; Zakharov, L. N.; Fronczek, F. R.; Slebodnick, C.; Lam, M.; Golen, J. A.; Bryant, W. S.; Mason, P. E.; Rheingold, A. L.; Ashraf-Khorassani, M.; Gibson, H. W., Bis(*m*-phenylene)-32-Crown-10-Based Cryptands, Powerful Hosts for Paraquat Derivatives. *J. Org. Chem.* **2005,** 70, (8), 3231-3241.